Supporting Information for

Directionally Interacting Spheres and Rods Form Ordered Phases

Wenyan Liu,[1,&,†] *Nathan A. Mahynski,*[2,&,#] *Oleg Gang,*[1,3,4*] *Athanassios Z. Panagiotopoulos,*[2*] *Sanat K. Kumar*[3]

[1]Center for Functional Nanomaterials, Brookhaven National Laboratories, Upton, NY

[2]Department of Chemical and Biological Engineering, Princeton University, Princeton, NJ

[3]Department of Chemical Engineering, Columbia University, New York, NY

[4]Department of Applied Physics and Applied Mathematics, Columbia University, New York, NY

Present Address

[†]Center for Research in Energy and Environment, Missouri University of Science and Technology, Rolla, MO

[#]Current address: Chemical Sciences Division, National Institute of Standards and Technology, Gaithersburg, MD

Corresponding Author

*E-mail: oleg.gang@columbia.edu; azp@princeton.edu

[&]These authors contributed equally to the work.

Calculation of effective particle sizes

The effective particle sizes were determined by the following equation:

$$D_{eff} = 2(R + T)$$

here R is the particle core radius, and T is the DNA shell thickness. T was approximated according to Daoud-Cotton Blob model[1] as:

$$T = R\left[\left(1 + k\frac{L_c}{R}\left(\frac{\sigma\nu}{l_k}\right)^{\frac{1}{3}}\right)^{\frac{3}{5}} - 1\right]$$

where $L_c = Nl$ is the contour length of ssDNA consisting of N nucleotides of segment length l = 0.65 nm; $l_k = 2l_p$ (persistence length $l_p \approx 1$ nm); σ is the tethering density that was estimated to be ≈ 0.2 chains/nm^2 here; k ≈ 1 is a constant; the excluded volume parameter ν can be estimated using Onsager's concept as $\nu = 1.5l_k^2 d_{eff}$, where the ssDNA can be considered as a charged cylinder chain with a length of Kuhn Length l_k and an effective diameter d_{eff} that was estimated to be ≈ 2 nm here. The values for R, N, T and D_{eff} are listed in Table S1

Table S1 Calculation of effective particle diameters

Particle radius *R* (nm)	**DNA length *N*** (nt)	**DNA shell thickness** (nm)	**Effective particle size D_{eff}** (nm)
3.0	12	3.6	13.2
3.0	20	5.4	16.8
3.0	30	7.4	20.8
3.0	35	8.3	22.6
3.0	50	10.7	27.4
4.35	12	3.9	16.5
4.35	20	5.9	20.5
4.35	30	8.1	24.9
4.35	35	9.1	26.9
4.35	50	11.8	32.3

Estimation of interparticle distances

The nearest neighbor center-to-center interparticle distances (d) in the assembled superlattices were calculated as:

$$d = D_{eff} + Z * N$$

where D_{eff} is the effective particle diameter (gold core and DNA shell); Z is the effective rise per base pair for rigid DNA motifs that link nanoparticle, considered here Z = 0.24 nm/bp based on the previous studies;[2,3] N is the total number of nucleotides along the length of a 6HB rod. The effective rise per base pair is lower than for nominal value for DNA (0.34 nm/bp) due to the off-axis attachment of a rod between nanoparticles, as revealed by our SAXS experiment and showed previously.[2,3] The comparison of the estimations with SAXS results indicate that for the 6HB rod Z is similar to the reported 0.24 nm/bp.

For the system $P_{6.0}$-S_{29} shown below, $d = 22.6 + 0.24 * 63 \approx 38\ nm$.

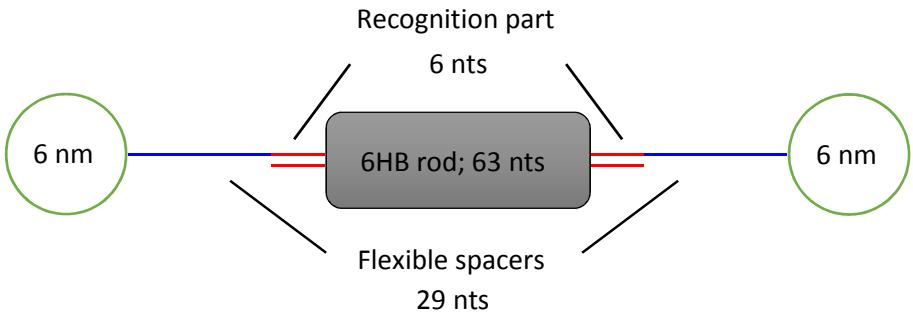

For the system $P_{6.0}$-S_{44} shown below, $d = 27.4 + 0.24 * 63 \approx 42.5\ nm$.

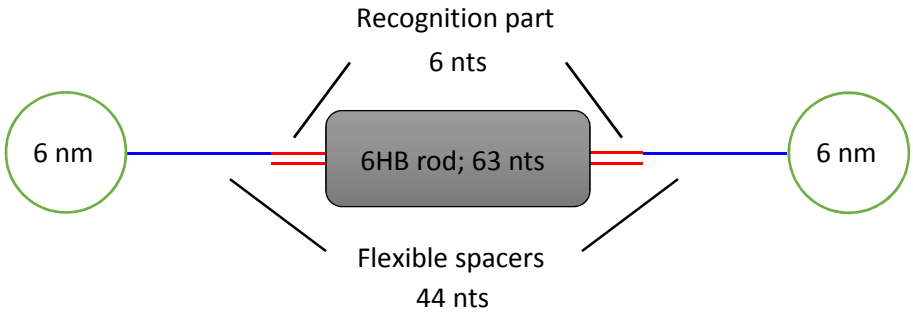

DNA sequences

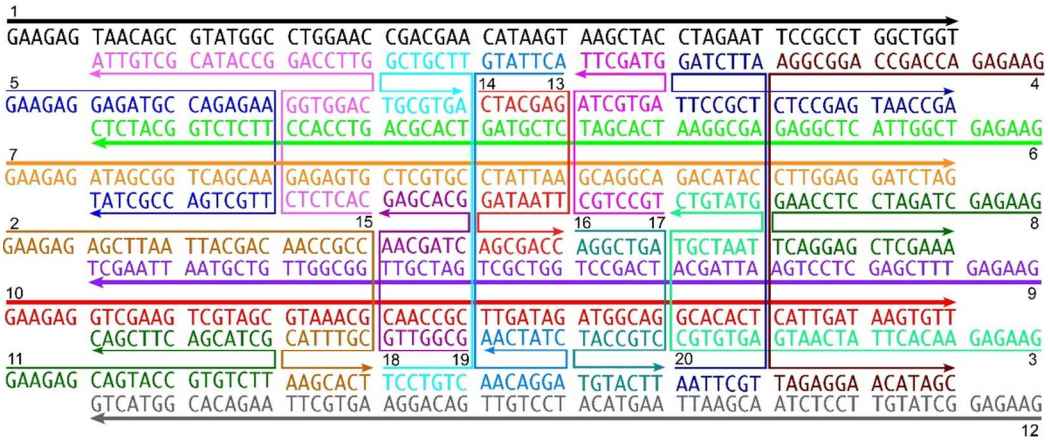

Figure S1. Strand structure for the 6HB rod. The 6HB rod is composed of 20 ssDNA strands that are indicated by the numbers and different colors. Both ends of the 6HB rod carry the same set of sticky ends that can hybridize with its complementary counterpart on the gold nanoparticle surface.

Gold nanoparticle-capping DNA

S6 (12mer)	5'-*CTCTTC*AAAAAA/3ThioMC3-D/-3'
S14 (20mer)	5'-*CTCTTC*AAAAAAAAAAAAAA/3ThioMC3-D/-3'
S24 (30mer)	5'-*CTCTTC*CTATGTGCTCGTCAGAAAAAAAA/3ThioMC3-D/-3'
S29 (35mer)	5'-*CTCTTC*CTATGTGCTCGTCAGAAAAAAAAAAAAA/3ThioMC3-D/-3'
S44 (50mer)	5'-*CTCTTC*CTATGTGCTCGTCAGAAAAAAAAAAAAAAAAAAAAAAAAAAAA/3ThioMC3-D/-3'

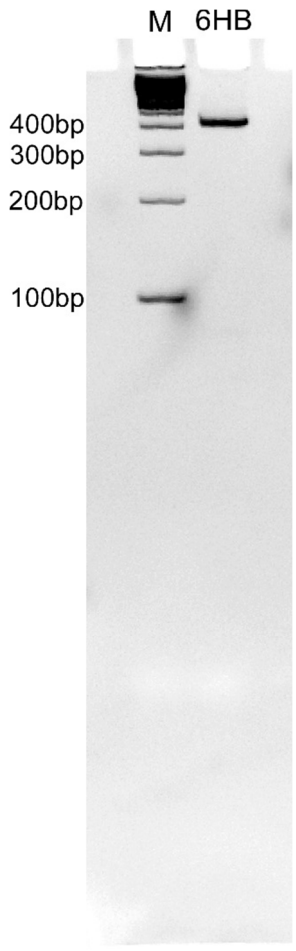

Figure S2. A 6% nondenaturing PAGE gel demonstrating the formation of the 6HB structure (size: 414bp). It is clear that the resulting 6HB rod appears as a single sharp band without any unwanted association or dissociation, and its mobility is in the expected range, relative to a ladder of linear duplex markers. These indicate that the 6HB rods constructed are stable and monodisperse under the experimental condition.

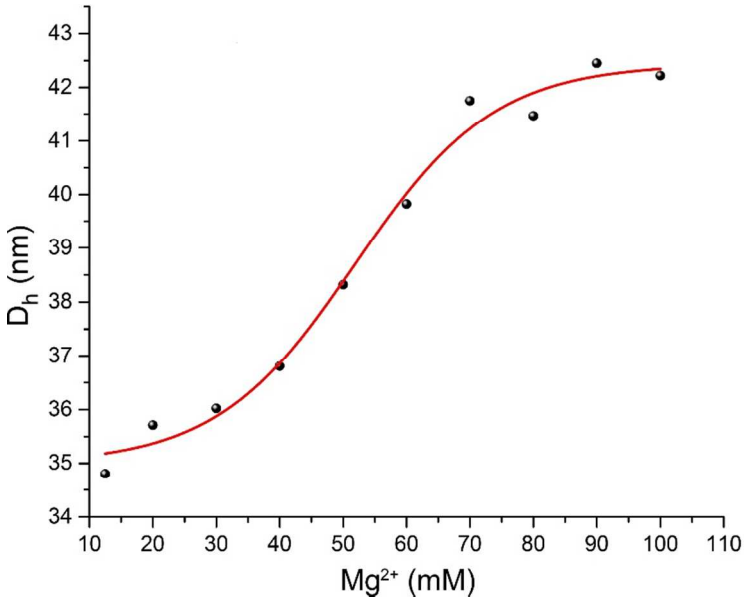

Figure S3. Salt stress dependence of the behavior of 6HB-gold nanoparticle conjugates. To investigate the impact of the salt stress on the weak non-specific interactions between the ends of two rods, one experimental system was prepared. The system is composed of 35-nt DNA modified 10 nm gold nanoparticles and 6HB linkers, which can link together through DNA hybridization. To avoid particle-particle interactions through 6HB linkers, the association ability of one side of the 6HBs has been eliminated by replacing the stick end sequence with short poly-T. The system was assembled by simply mixing 6HBs and gold NPs in 1 × TAE buffer (12.5 mM Mg^{2+}) at a ratio of 100:1, followed by a thermal annealing from 50°C to RT in a course of 36 hours. After annealing, the sample underwent a further purification process to remove the excess of 6HBs. The samples were characterized by using Dynamic Light Scattering (DLS). In each measuring step, the concentration of Mg^{2+} was adjusted to reach the target concentration. The result clearly shows that the particle size got increased non-linearly with the increase of the Mg^{2+} concentration. This may be due to the fact that although the sample was purified, there were still some free 6HBs in the solution. Therefore, as the salt concentration was increased, the repulsive forces among the 6HBs got reduced, causing them started to binding on the particle surfaces, which resulted in the increase of the particle size. However, with the decrease of the numbers of the free 6HBs in the solution, there are no many 6HBs available to bind on the particle surface, leading to the speed of the increase of particle size to slow down. Thus, the result indicates that the salt stress indeed has some impact on the size of the 6HB-gold nanoparticle conjugates, possibly, via an attachment of additional 6HBs to the 6HB-gold nanoparticle conjugates, as driven by Mg^{2+}-promoted attraction of non-complementary ends of 6HBs.

Additional systems: 6HB and 8.7 nm gold NP

In addition to the 6 nm gold core nanoparticles (NPs), we also investigated the assembly of NPs with 8.7 nm core using the same 6HBs as linkers. In the first studied system, the NPs were functionalized with thiolated 35-nt ssDNA containing a 29-nt flexible spacer ($P_{8.7}$-S_{29}). The NP aggregates were formed by mixing the 6HB linkers and the NP-DNA conjugates in 1×TAE/Mg^{2+} buffer at a ratio of 20:1 (6HB linkers: NP), followed by a thermal annealing procedure, as discussed in the method section. The comparison between experimental structure factors *S(q)* data (green curve) and calculated diffraction pattern (blue curve) reveals the formation of not so well-defined FCC crystal after the first annealing (Fig. S4a). To explore the possibility of increasing the quality of the assembled crystal structure, the annealed sample was subjected to the same thermal annealing process after removing the supernatant and subsequently refilling the capillary with the same amount of the 6HB linkers, as used for the initial experiment. *S(q)*, shown as the red curve in Figure S4a, clearly demonstrate significantly improved degree of crystallinity of FCC phase after further annealing. These results indicate that for the larger NPs, a higher amount of 6HB linkers is needed in order to form well-defined crystals. However, due to the annealing procedure used in this experiment, the most suitable linker/NP ratio for this system could not be determined precisely, it is on order 30:1.

In the next step, we examined two more systems based on 8.7 nm NPs. The DNA-NP conjugates were produced by coating the NP with thiol-modified 50-nt ssDNA containing a 44-nt flexible spacer. The two systems were prepared by mixing 6HB linkers and DNA-NP conjugates together in 1×TAE/Mg^{2+} buffer at a ratio of 30:1 and 40:1 respectively (denoted as $P_{8.7}$-S_{44}-R_{30}, and $P_{8.7}$-S_{44}-R_{40}, respectively), and subsequently undergoing a thermal annealing process (see method section). Figure S4b illustrates the SAXS-revealed structure factors *S(q)* for both systems. We observed for both $P_{8.7}$-S_{44}-R_{30} and $P_{8.7}$-S_{44}-R_{40} systems that *S(q)* peak positions and relative intensities match well the calculated pattern for the FCC lattice (blue curve in Figure S4b). However, the comparison of the results with the one shown by the red curve in Figure S4a,

indicate somewhat decreased degree of crystallinity. This maybe indicates that more titrations are needed as well as more complex phase formation process that requires multiple annealing for particle with larger binding area.

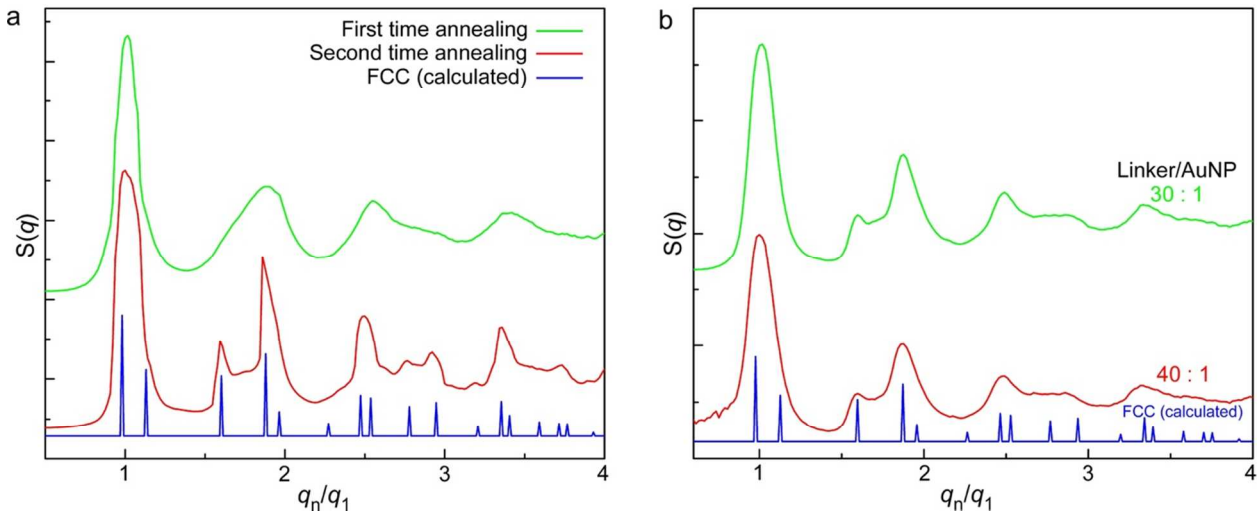

Figure S4. SAXS-obtained structure factors *S(q)* for 8.7 nm core NP assemblies directed by 6HB rod linkers. **(**a) Ratio-dependent SAXS extracted structure factors for two-step annealing. The NPs were functionalized with the thiolated 35-nt DNA. (b) Ratio-dependent *S(q)* for the system containing 50-nt DNA coating NPs.

(1) Hariharan, R.; Biver, C.; Mays, J.; Russel, W. B., Ionic Strength and Curvature Effects in Flat and Highly Curved Polyelectrolyte Brushes. *Macromolecules* **1998,** *31*, 7506-7513.

(2) Auyeung, E.; Cutler, J. I.; Macfarlane, R. J.; Jones, M. R.; Wu, J.; Liu, G.; Zhang, K.; Osberg, K. D.; Mirkin, C. A., Synthetically Programmable Nanoparticle Superlattices Using a Hollow Three-Dimensional Spacer Approach. *Nat. Nanotechnol* **2012,** *7*, 24-28.

(3) Chi, C.; Vargas-Lara, F.; Tkachenko, A. V.; Starr, F. W.; Gang, O., Internal Structure of Nanoparticle Dimers Linked by DNA. *ACS Nano* **2012,** *6*, 6793-6802.